SINTEF F23783- Restricted

Report

Combustion and NOx formation in silicon pilot furnace

Experiments and modelling

Author(s)
Jan Erik Olsen
Ingeborg Solheim, Balram Panjwani & Stefan Andersson

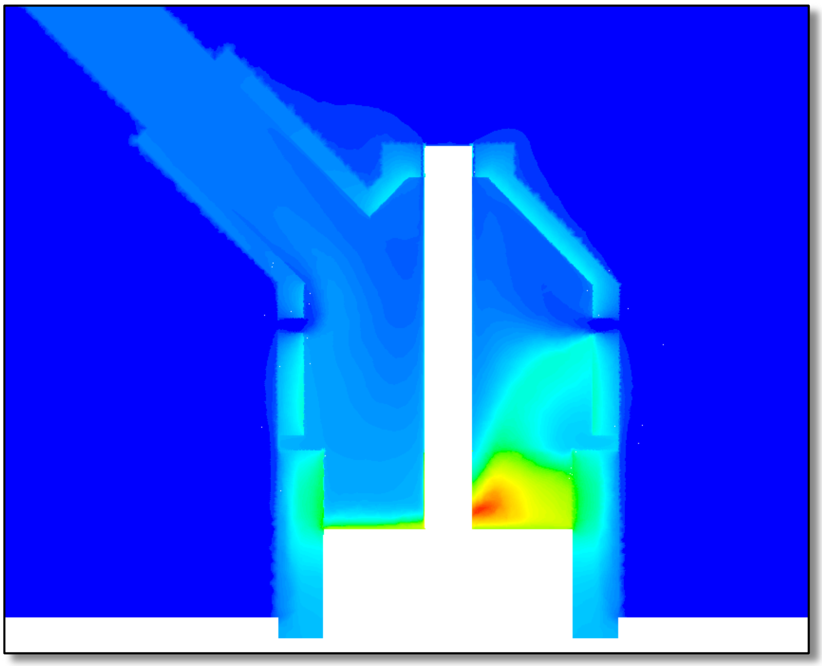

SINTEF Materials and Chemistry
Process Technology
2012-11-30

SINTEF Materialer og kjemi
SINTEF Materials and Chemistry

Address:
Postboks 4760 Sluppen
NO-7465 Trondheim
NORWAY

Telephone:+47 73593000
Telefax:+47 73597043

info.mk@sintef.no
www.sintef.no/mk
Enterprise /VAT No:
NO 948007029 MVA

KEYWORDS:
NOx
CFD
Pilot furnace
Modelling
Measurements
Ferrosilicon

Report

Combustion and NOx formation in silicon pilot furnace

Experiments and modelling

VERSION
1.0

DATE
2012-11-30

AUTHOR(S)
Jan Erik Olsen
Ingeborg Solheim, Balram Panjwani & Stefan Andersson

CLIENT(S)
FFF

CLIENT'S REF.
Jacob Steinmo

PROJECT NO.
805674

NUMBER OF PAGES/APPENDICES:
34 incl.1 Appendix

ABSTRACT

Pilot scale experiments and model validation have been conducted to investigate the effect of air supply and charge characterististics on NOx formation and to assess the accuracy of CFD models with respect to predictions of NOx emissions. The experiments show that NOx emission seems to decrease when using wet raw materials (charcoal and wet wood chips), compared to using dry raw materials (coke and dry wood chips). The model validation shows that all trends are picked up by the model, and the NOx calculations can be used for assessment of proposed design changes on furnaces. However, the quantitatively the model does not predict the NOx emissions fairly well. The model can be improved by considering more realistic boundary conditions, a transient model concept and/or improved reaction schemes. $SiO+H_2O \rightleftarrows SiO_2+H_2$ should be considered in future work.

PREPARED BY
Jan Erik Olsen

SIGNATURE

CHECKED BY
Are Simonsen

SIGNATURE
Are J. Simonsen

APPROVED BY
Webjørn Remen

SIGNATURE

REPORT NO.	ISBN	CLASSIFICATION	CLASSIFICATION THIS PAGE
SINTEF F23783	ISBN	Restricted	Restricted

Document history

VERSION	DATE	VERSION DESCRIPTION
1.0	2012-12-19	First version

Table of contents

1 INTRODUCTION

Nitrogen oxides (NO and NO_2) often referred to as NOx, play an important role in the atmospheric reaction that creates fine particle and ozone smog. NOx emissions also contribute to a variety of year-round environmental problems, including acid rain, eutrophication (stimulated growth of algae and bacteria) and bronchia sufferings. These effects have a marked negative impact on the health of wildlife, vegetation and human population. The main source of NOx emissions is shipping and car traffic. In Norway the land based industry is responsible for 10% of the emissions. The ferrosilicon industry emits 50% of this or 5% of the total Norwegian emissions. Fuel NOx is emitted from shipping and car traffic, while in ferrosilicon production thermal NOx is emitted. Thermal NOx is formed when nitrogen and oxygen are present at high temperatures.

Ferrosilicon is produced in submerged arc furnaces (SAF) where ore (silica) and carbon (coke, coal, etc.) are mixed into a charge and react when electric energy is supplied through electrodes. The reactions produce alloys and an energy rich off-gas. The alloys sink to the bottom and are collected through a tapping process. Hot process gas rises upwards through the charge surface and into a furnace hood. Simultaneously air is sucked into the hood through various open areas due to the pressure drop. The air and process gas reacts in a combustion process and produces an off-gas potentially containing harmful substances. This is illustrated in Figure 1. In a ferrosilicon furnace the process gas emerging from the charge surface mainly consists of CO with some SiO, water vapour and volatiles. The combustion taking place between process gas and air in the furnace hood creates high temperature with potential for formation of thermal NOx. As stated above, the emission of NOx is harmful and authorities are continuously increasing the restrictions and cost of NOx emissions on the industry. Reduction of NOx emissions is thus important for production cost, license to operate and reputation.

NOx formation depends on how air is mixed with process gas and the temperature levels reached by the resulting combustion. Supply and distribution of air strongly depends on design of furnace hood and off-gas channels. Due to high installation cost of furnace hoods, it is not economically feasible to apply a trial end error approach with different design. Mathematical modeling by computational fluid dynamics (CFD) provides a more affordable solution to design optimization. CFD can also give an insight to conditions in the furnace hood which is difficult to observe and measure due to the hostile environment. Motivated by this, a CFD modeling concept accounting for the governing mechanisms in the furnace hood have been developed to study the effect of operations and design on NOx emissions and other performance indicators. The modeling concept and results are presented below.

Validation data for the CFD model was created by a furnace experiment at pilot scale. The experiment provided both validation data and insight to the governing parameters of the combustion process and NOx formation.

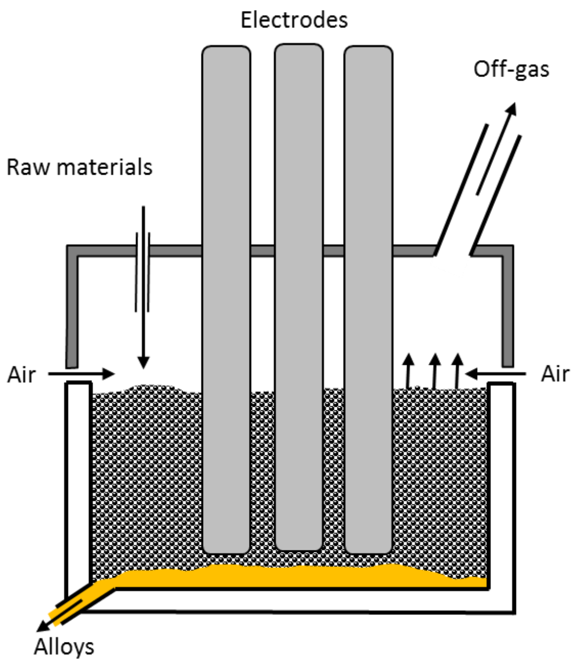

Figure 1: Sketch of submerged arc furnace

2 PILOTSCALE EXPERIMENT

2.1 Furnace

The experiment was carried out in a 440 kVA single phase furnace with adjustable current and voltage supply. The furnace can be operated with both AC and DC power supply. Maximum DC current is 8000 A and maximum voltage is 300 V. Maximum AC current is 5700A and maximum voltage is 215 V. For this experiment AC was chosen, in order to operate the furnace as similar as possible as previous pilot scale experiments[1]. The furnace hood is connected to an off gas system, and equipment for monitoring composition and temperature of the gas is installed. Afilter for collecting coarse and fine dust particles is added at the end-of-pipe. .

The off-gas hood is designed with the intention to have several controllable false air inlets into the combustion chamber, and at the same time be able to perform stoking and charging operations. A sketch and a picture of the furnace are shown in Figure 2.

The furnace body is constructed with an outer steel mantle which is divided horizontally just below the tap hole. The top is sectioned vertically in order to be able to dismantle the furnace pot into two halve sections. This particularly design permits filling of the furnace with epoxy after ended experiment such that the moulded mass can be removed in one piece; this is a very useful technic in post experimental studies. For these study the entire furnace in slices, and subsequently drill out samples from decided positions for analysis. The figure below shows a typical cross section of the furnace after ended experiment and a schematic overview of the different reaction zones.

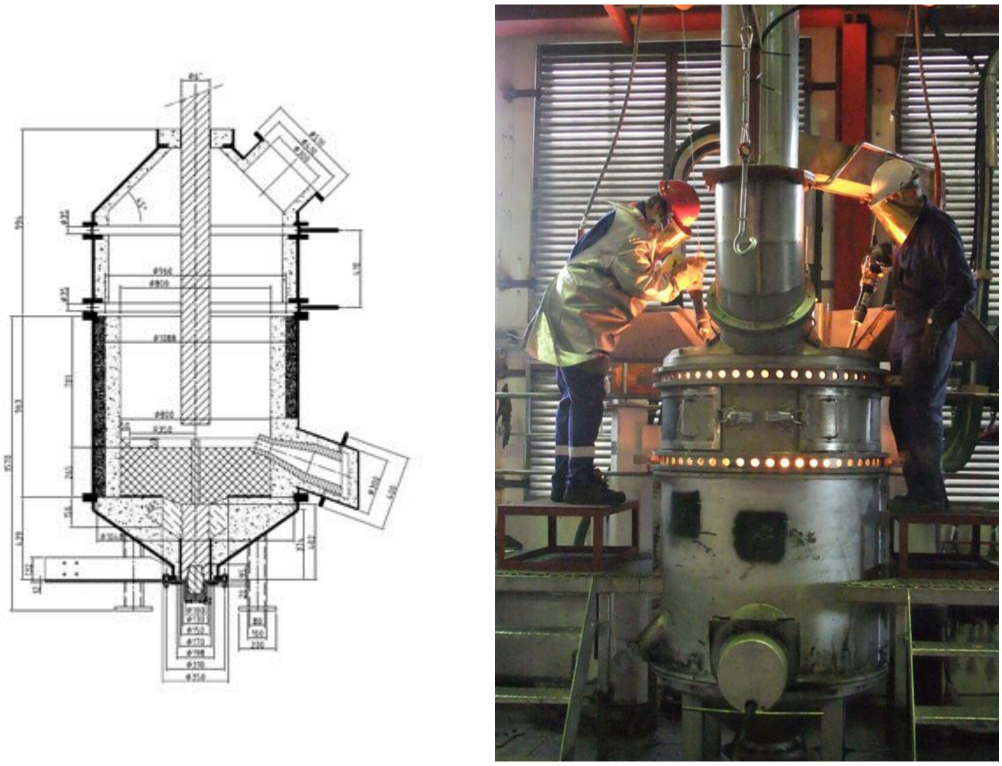

Figure 2: The figure shows a sketch of the furnace and a picture of the furnace in action.

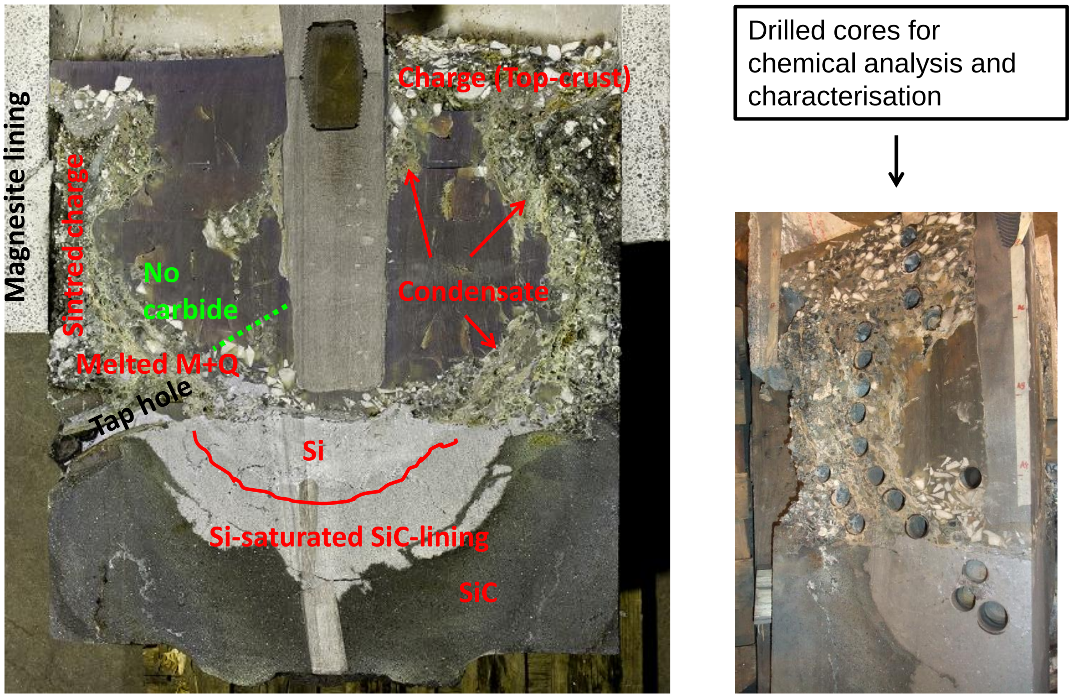

1

Figure 3: The figure shows a typical cross section of the furnace after ended experiment.

The bottom lining was stamped with conductive SiC. In the bottom, a graphite electrode was connected to the power via copper tracks and a copper bolt below the furnace. In the side lining an Al_2O_3-based paste was used, and the gap between the steel mantle and side-lining was filled with a 5 cm thick layer of silver sand (SiO_2). A graphite electrode of 6 inches (15 cm) is installed from the top, and the electrode can be adjusted up and down.

2.1.1 Raw materials

The raw materials used for this experiment was quartz (3-25 mm), charcoal (3-15 mm) and coke (3-15 mm). In addition wood chips (20-50 mm), was added to increase charge permeability and to "ventilate" the charge. The raw material mix started with a carbon cover of 80 %, gradually increased up to 97 %.

All raw materials were supplied by Elkem. Delivery conditions for the quartz were that source and analysis were confidential and are therefore not presented in this report. The analysis of coke and wooden chips is given in Table 1.

Table **2** shows the fraction of raw materials used and the measured humidity.

Table 1: Chemical analysis of raw materials used in the melting experiment

Raw material	FixC %	Volatiles %	Ash %	Ash-analysis										
				SiO_2 %	Al_2O_3 %	CaO %	Fe_2O_3 %	K_2O %	MgO %	MnO %	Na_2O %	P_2O_3 %	SO_3 %	TiO_2 %
Coke	92,1	5,91	1,99	41,4	25,3	4,4	11,1		2,8					
Charcoal	51,6	38,9	1,18	48,6	20,9	4,0	11,3	0,5	2,9					0,88
W.chips	25,0	72,9	0,23	0,052	0,004	0,431	0,019	0,132	0,049	0,027	0,002	0,022	0,015	0,001

Table 2: Humidity and size fractions of raw materials used

	Fraction (mm)	Humidity (%)
Quartz	3-25	0,1
Coke	3-15	0,97
Charcoal	3-15	8,9
Wooden chips wet	20-50 (~)	42,1
Wooden chips dry	20-50 (~)	5,6

The analytical data presented in Table 1 and
Table **2** is used as a basis for the charge mix of raw materials.

2.1.2 Furnace operation

The plan was to operate the furnace as similar as possible to a previous pilot scale experiments[1]. Initially, the pilot was to be operated at a constant effect of approximately 160 kW, but during the experiment 180 kW was found to be more adequate for the current set up. AC power supply was chosen, and the effect was kept constant by adjusing the current.

Through the experiment, after steady conditions was achieved, several trials where performed. In each trial a set of parameters were changed and corresponding off gas compositions measured. The parameters tested was position of false air inlet (upper or lower perforated ring in the hood open) and humidity/volatility of raw materials (wet or dry).

Electrical parameters:

Effect: 160 kW,Current: 4 kA, Voltage: 40 V

Tapping schedule:

After each 250 kWh: the electrode has to be gradually lowered to the bottom of the empty furnace during the tapping operation. The current has to be shut off after ended tapping, for a quick stoking operation of the furnace.

Stoking and charging:

Stoking with pneumatic tools is performed immediately after tapping. The electrode has to be raised (5 cm) after ended stoking before the furnace can be switched on again. After the power is switched on the furnace have to be charged rapidly with raw material up to ¾-level, and then gradually be refilled up to normal level (about 20 cm from upper pot-edge)

Data logging:

Different parameters, like electrode position, stoking and charging activity was manually logged. Weight of SiO_2 was measured after each tapping. Power supply and off gas analysis results were logged continuously.

Off gas measurements:

TESTO 350XL and a FTIR was used for the off gas measurements. The furnace flowsheet for the off gas system is shown in the figure below. Test points for off gas temperature, flow and chemical analysis are also indicated. Dust was measured by a NEO optical cell.

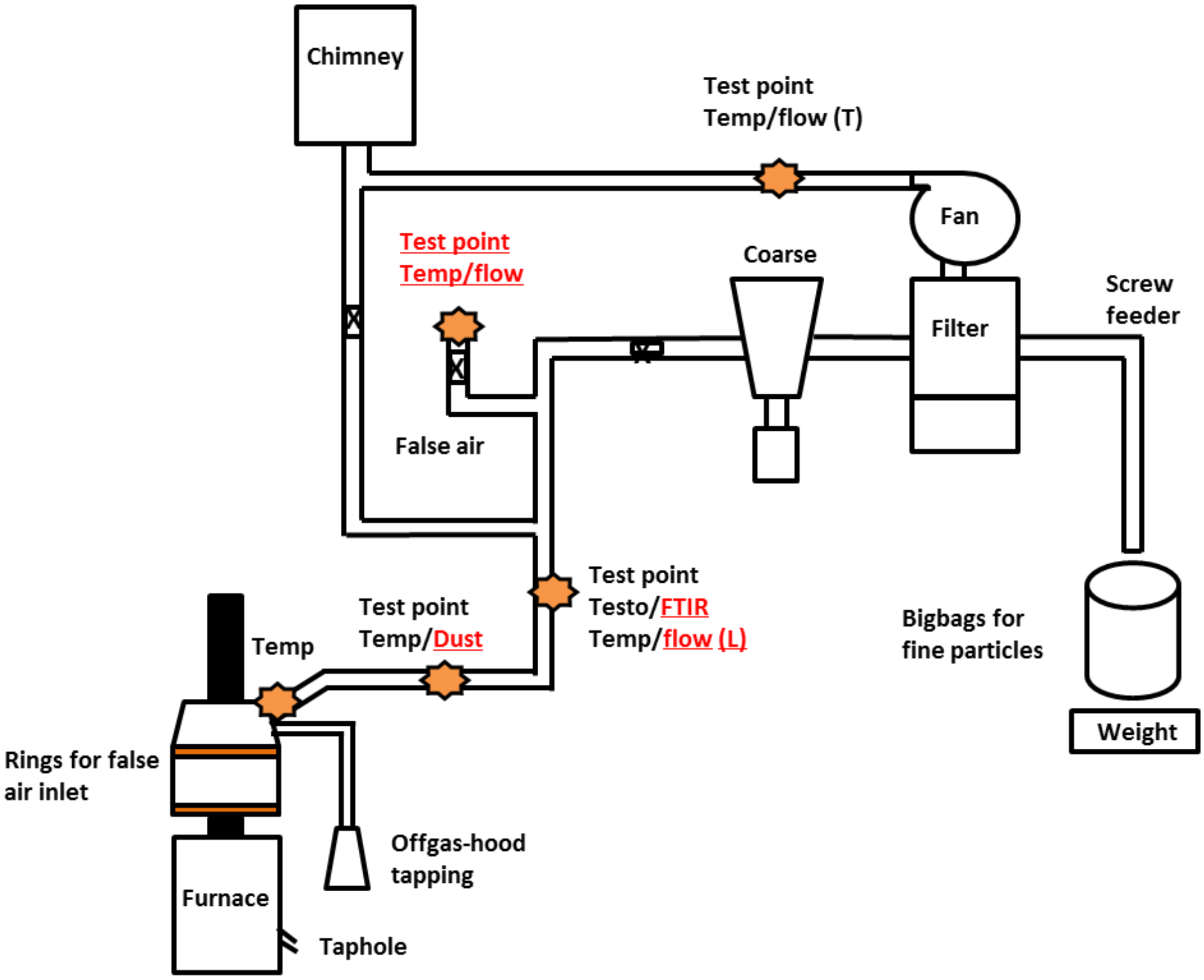

Figure 4: Furnace flow sheet for the off gas and the filter bag house system.

2.1.3 Trial matrix

The table below shows the test parameter setup during each trial/run. Each run was finished with a tapping followed by recharging of new raw materials for the next run. Tap 1 corresponds to metal from run 1, tap 2 to run 2 etc…

Table 3: Overview of parameter setup during each run. W = wet, D = dry, U = upper, L = lower.

Run	Raw material	False air inlet
1	W	U
2	W	L
3	D	L
4	D	U
5	W	L
6	D	L
7	W	U
8	D	U
9	W	U
10	D	U
11	W	L
12	D	L
13	W	U

Wet raw material corresponds to
charcoal (8,9 % humidity / 38,9 % volatiles) and wet wood chips (42,1 % humidity / 72,9 volatiles).

Dry raw material corresponds to
coke (0,97 % humidity / 5,91 % volatiles) and dry wood chips (5,6 % humidity / 72,9 % volatiles).

Upper false air inlet is ~70 cm above charge level.
Lower false air inlet is ~20 cm above charge level.

2.2 Results

2.2.1 Silicon metal and fumed silica

The silicon pilot furnace was operating for 39 hours, producing with a silicon yield of 53 %. It was tapped 13 times, giving a total of 58,2 kg's of silicon metal and 49,2 kg of fumed silica. The results from the furnace operation are summarized in the table below. Of the 39 hours furnace operation, 15 was spent on preheating and charging up the furnace. The last 24 hours of operation was accomplishment of the experiments i.e the trial matrix. The graphs presented in the following are results obtained during this periode.

Table 4 Results from the furnace operation. The * marks time for joining of new electrode.

Tap nr	Time from start (hh:mm)	Time between tapping	Metal produced kg	Silica produced kg	kWh pr production period	Furnace effect kW	kWh/kg Si
1	0	0	0	4	1307	150	-
2	02:00	2	0	0,8	391	150	-
3	03:50	1,8	0	2	247	150	-
4	05:30	1,6	0	2,2	258	170	
5	07:10	1,6	0	2,7	242	170	-
6	10:15	3*	5,8	4	Not noted.	175	
7	12:10	2	7,3	4,14	263	180	36
8	13:30	1,3	6,8	3,2	171	180	25
9	15:15	1,7	9,8	6,3	270	180	26
10	17:00	1,7	4,9	3,9	269	180	55
11	19:15	2,25	12,9	7,2	335	180	26
12	22:00	2,8	5,3	6	394	180	74
13	23:30	1,5	5,5	2,7	231	180	42

2.2.2 Current and voltage

As mentioned earlier the operational strategy was to keep the average effect at 180 kW by adjusting the current. Periods with zero-effect correspond to tapping of the furnace. Relevant data from the current and voltage measurements are given in Figure 5.

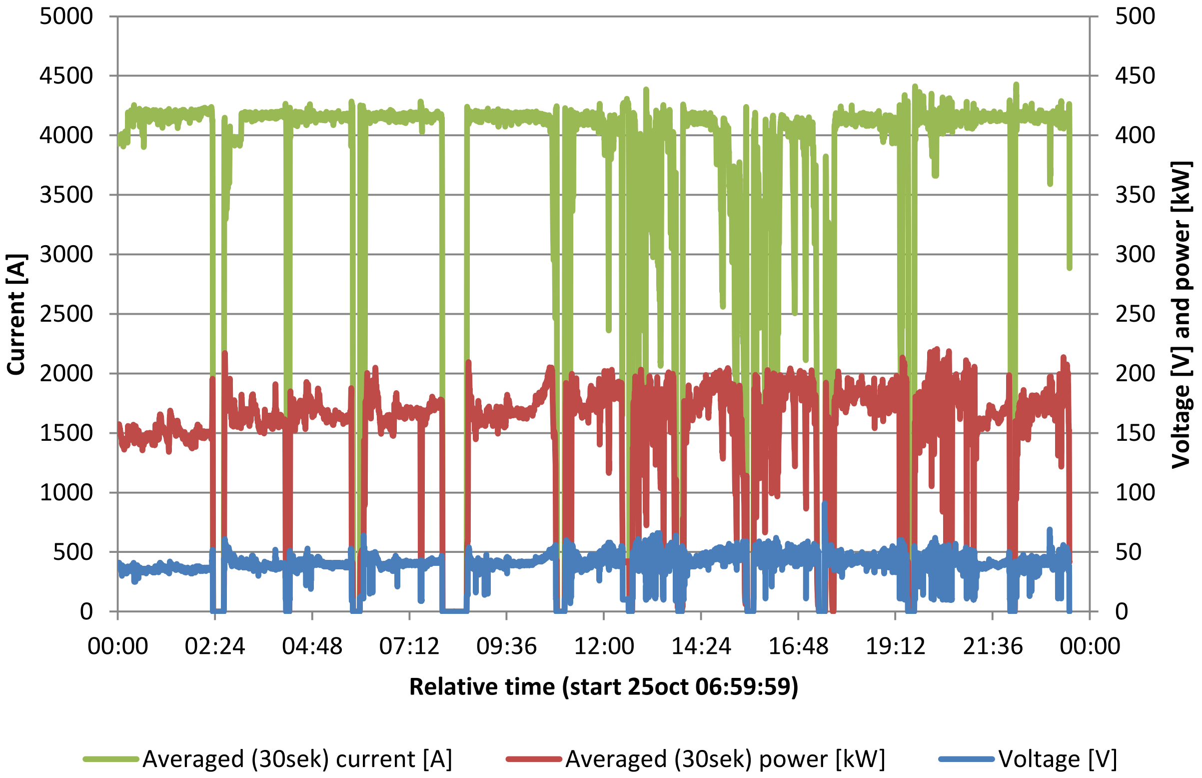

Figure 5: Current, voltage and power for the last 24 hours of the experiment.

2.2.3 Off-gas measurements

Measurements of NOx (NO+NO_2) during the trial matrix periode (last 24 hours) are shown in figure 6. Measurement of H2O and CH4 is compared with NOx in respectively figure 7 and 8.

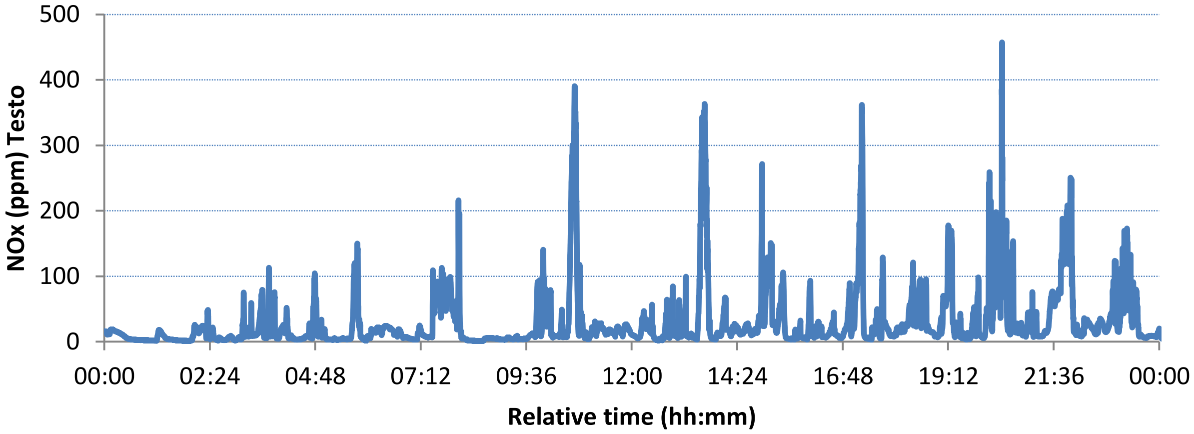

Figure 6: NO and NO_2, measured and compared for results form Testo and FTIR, for the last 24 hours of the experiment.

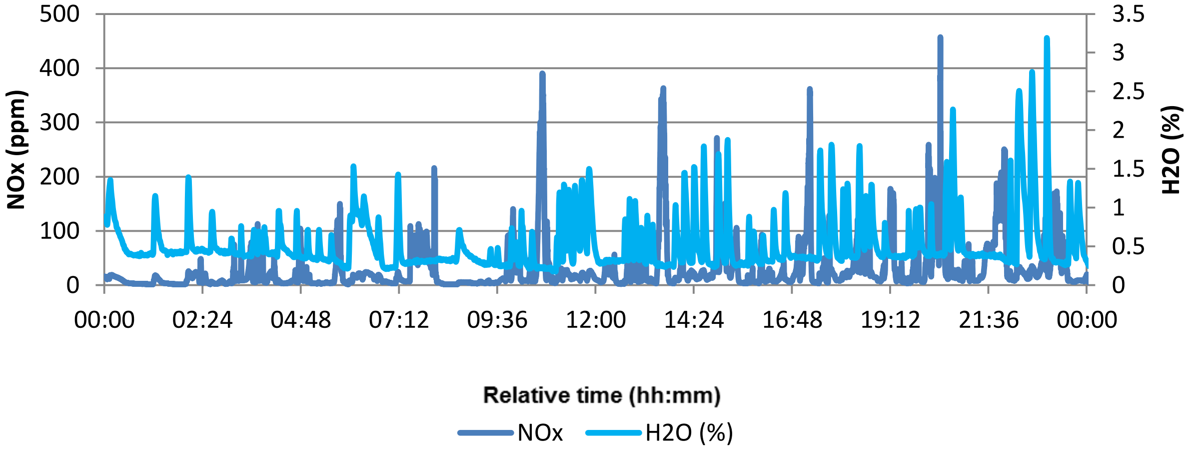

Figure 7: NOx and H_2O measured and compared for the last 24 hours of the experiment.

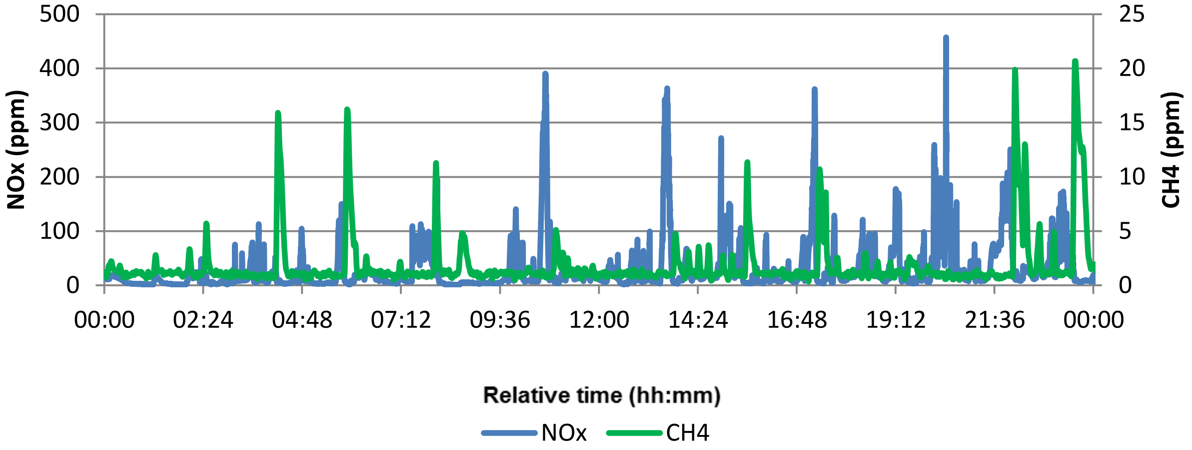

Figure 8 NOx and CH_4 measured and compared for the last 24 hours of the experiment.

2.2.4 Dust measurements

The dust was measured by a NEO optical cell. Due to problems with the measure range (far above the original calibration), there is no data logged for the first 7 hours.

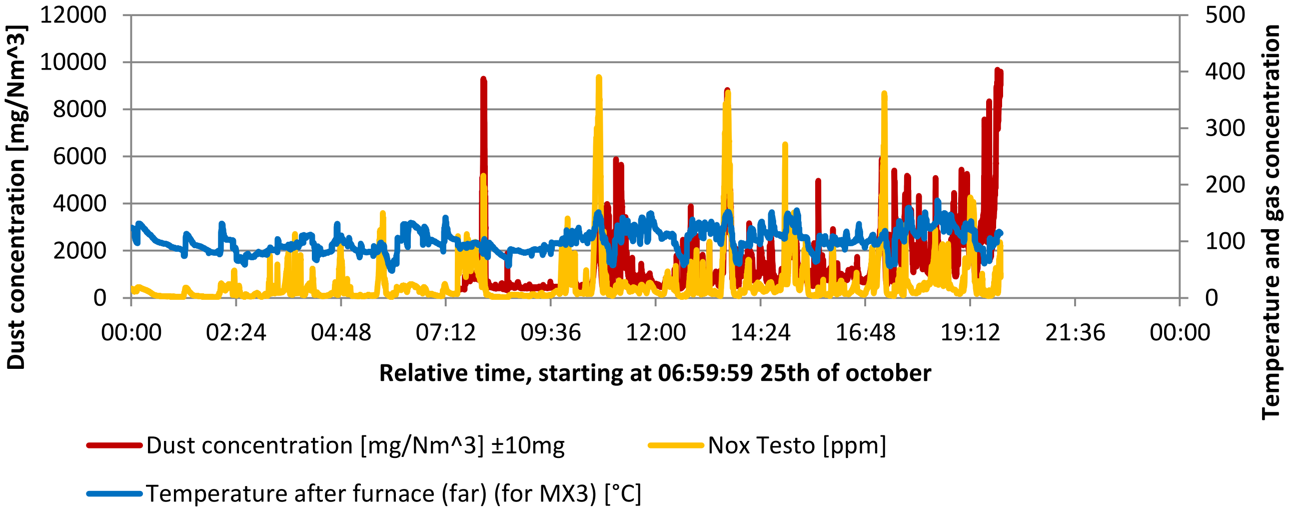

Figure 9: Dust concentration compared to NOx concentration (last 24 hours).

2.2.5 NOx summarized

4 runs representing 4 different combinations of parameters, was selected to compare the average NOx emission within each run. The results are presented in the bar graph beneath. W= wet raw materials, D = dry raw materials, U = upper false air inlet, L= lower false air inlet.

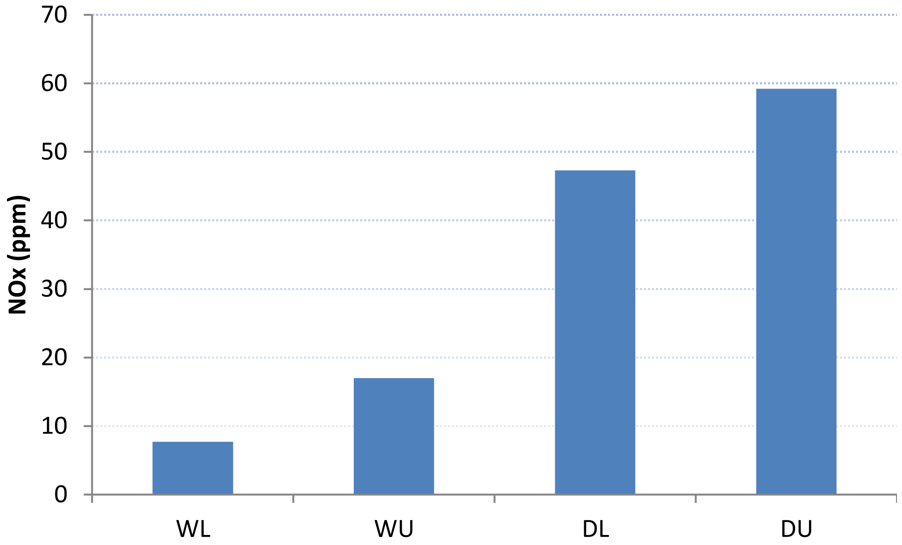

Figure 10: Average NOx emission within run 2, 6, 7and 8, representing 4 different combinations of parameters: Run 2= WL, run 6 = DL, run 7 = WU and run 8 = DU.

2.3 Conclusion pilot scale experiment

The NOx emission seems to decrease significant by using wet raw materials (charcoal and wet wood chips), compared to using dry raw materials (coke and dry wood chips). This is probably due to addition of both water and hydrocarbons in the gas above the charge. Water evaporation contributes to decrease the gas temperature. The hydrocarbons will probably consume the oxygen for other competeting reactions.

3 CFD MODEL FOR NOx EMISSIONS AND FURNACE HOOD CONDITIONS

The combustion process in the furnace hood of a ferrosilicon furnace is dominated by transient and turbulent flames, high temperatures and dusty conditions. The adiabatic flame temperature of the process gas may peak around 2500°C to 2800°C. The gas is composed of species introduced from the process gas and air intakes as well as the product of their reactions, including radicals. The reaction rates depend on temperature and mixing which again depends on turbulence. Turbulent length scales in industrial furnaces vary from millimeters to meters.

Ideally such a process should be modelled with a transient turbulence model (e.g. Large Eddy Simulations) and detailed chemistry. Due to large variations in physical and turbulent length scales in industrial furnaces, modelling simplifications are required in order to reduce the computational cost. Thus steady-state simulations with time averaged turbulence models and reduced reactions schemes are often applied. The calculation of temperature field and gas composition makes it possible to estimate the NOx-emissions from the process.

Table 5: Species accounted for in model

Process gas	Air	Products
CO	N_2	CO_2
SiO	O_2	SiO_2
H_2O		NO
		O
		OH

3.1 Modelling concept

Describe model:

The applied modelling concept conserves mass and momentum by solving the continuum equation and the Navier-Stokes equations [2]. The turbulent viscosity added to the Navier-Stokes equations is closed by the standard k-ε turbulence model [2]. Together with the ideal gas law, these equations provide the density, pressure and velocity field together with turbulence parameters. Conservation of energy E is assured by the energy equation

$$\frac{\partial}{\partial t}(\rho E) + \nabla \cdot \left(\vec{v}(\rho E + p)\right) = \nabla \cdot \left(k_{\text{eff}} \nabla T - \sum_j h_j J_j \right) + S_{react} + S_{rad} \tag{1}$$

where the first two terms on the right hand side represent energy transfer due to conduction and species diffusion. The last two terms are source terms due to the heat of chemical reactions and radiation. The energy is defined as

$$E = h - \frac{p}{\rho} + \frac{v^2}{2} \tag{2}$$

Here h is sensible enthalpy. Due to the high temperatures seen in these furnaces, heat transfer by radiation is significant. The Discrete Ordinance model (DO-model) [3] is applied for conservation of radiation heat. It solves a transport equation accounting for absorption and scattering in the gas with boundary conditions for surface emissivity at solid surfaces. The energy equation together with input from radiation and reaction heat provides the temperature field.

Conservation of species is accounted for by the species conservation equation

$$\frac{\partial}{\partial t}(\rho Y_i) + \nabla \cdot (\rho \vec{v} Y_i) = \nabla \cdot (\rho D_i \nabla Y_i) + R_i \tag{3}$$

where Y_i is the mass fraction, D_i is the diffusion coefficient and R_i is the net rate of production of species i by chemical reactions. This equation is solved for N-1 species where N is the total number of fluid phase chemical species present in the system. Since the mass fraction of the species must sum to unity, the N^{th} mass fraction is determined as one minus the sum of the $N - 1$ solved mass fractions. The term for production of species i, R_i, is given by stoichiometric coefficients and rate coefficients according to the Arrhenius expression which for a forward reaction is given by

$$k_{f,r} = A_r T^n e^{-E_r/RT} \tag{4}$$

For modelling the combustion-turbulent interaction a combustion model is required. In the present study an Eddy Dissipation Concept (EDC) model is applied. The EDC model is based on turbulent energy cascade model. The energy cascades from the large-scale structures to smaller scale structures. This process continues until structures are sufficiently small and they can't transfer energy further down. The EDC model assumes that the chemical reaction occurs on these smaller dissipative structures. The length and time scales of the fine structures are on the same order as the Kolmogorov length scale. Combustion at these fine scales is assumed to occur as a constant pressure Perfectly Stirred Reactor (PSR) [4] , with initial conditions taken as the current species and temperature in the cell. Reactions proceed over the time scale, governed by the Arrhenius rates of Equation (4).

The gas species tracked in the model is CO, SiO and H_2O originating from the furnace crater, O_2 and N_2 from surrounding air and CO_2 and SiO_2 which are products of the reactions. In reality there is an extensive reaction scheme governing the combustion process. However, a simplified or reduced scheme has been investigated initially. This is listed in Table 6. In such reduced schemes, the reaction kinetics needs to be tuned for the typical conditions of interest. Radicals, such as O and OH, and full reactions schemes may also be accounted for as discussed below. In addition NOx is tracked as NO. With a reduced reaction scheme without radicals, NOx formation can be estimated in a post processing operation with the following source term for NOx formation [5]:

$$\frac{d[\mathrm{NO}]}{dt} = 2k_{f,1}[\mathrm{O}][\mathrm{N_2}]\frac{1 - \dfrac{k_{r,1}k_{r,2}[\mathrm{NO}]^2}{k_{f,1}[\mathrm{N_2}]k_{f,2}[\mathrm{O_2}]}}{1 + \dfrac{k_{r,1}[\mathrm{NO}]}{k_{f,2}[\mathrm{O_2}] + k_{f,3}[\mathrm{OH}]}} \tag{5}$$

where the different constants $k_{x,n}$ are rate coefficients [5]. NO is tracked by Eq.(3) with i=NO. The concentration of O-atoms is estimated based on the O_2 concentration. The equilibrium approach of Westenberg [6] is applied:

$$[\mathrm{O}] = 3.97 \cdot 10^5 T^{-1/2}[\mathrm{O_2}]^{1/2} e^{-31090/T} \tag{6}$$

The [OH] concentration is estimated by [7]

$$[\mathrm{OH}] = 2.129 \cdot 10^2 T^{-0.57}[\mathrm{O_2}]^{1/2}[\mathrm{H_2O}]^{1/2} \tag{7}$$

If applying a full reaction scheme, calculation of NOx formation is coupled with the other reactions as described below. It is possible to apply both a laminar and turbulent approach on the NOx estimation. In a laminar approach the effect of turbulence is neglected and the source term in NOx transport equation.

$$R_{thermal,NO} = M_{w,NO}\frac{d[\mathrm{NO}]}{dt} \tag{8}$$

Accounting the turbulence for the NO_x rate can be based on either moment methods or probability density function (PDF) techniques. ANSYS FLUENT uses the PDF approach. A single or joint-variable PDF in terms of a normalized temperature, species mass fraction, or the combination of both is used to predict the NOx emission. A detailed description is found in the ANSYS FLUENT manual. The source term in NOx transport equation is

$$\bar{R}_{thermal,NO} = \int R_{thermal,NO}\,(T)P(T) \tag{9}$$

The reduced reaction scheme and post processing procedure for NOx formation described above, gives a computationaly efficient model for studying combustion and NOx formation in a furnace. Alternatively we might use a full reaction scheme with radicals and NO reactions. In doing so, a reaction scheme accounting for the relevant reactions and species need to be defined. In the following study, the full reaction scheme has been chosen as given by Table 7 [8, 9].

Table 6: Reduced reaction scheme with kinetic parameters[1] in Kelvin, cal/mol, cm^3

Reactions	A_r	n	E_r
1. $2CO + O_2 \rightarrow 2CO_2$	2.24E+18	0.00	4776
2. $2SiO + O_2 \rightarrow 2SiO_2$	1.00E+18	0.00	0.24

Table 7: Full reaction scheme with kinetic parameters in Kelvin, cal/mol, cm^3

Reactions	A_r	n	E_r
1. $O_2+CO \rightleftarrows O+CO_2$	2.50E+12	0.00	47800
2. $2OH \rightleftarrows O+H_2O$	3.57E+04	2.40	-2110
3. $OH+CO \rightleftarrows H+CO_2$	4.76E+07	1.23	70
4. $H+O_2 \rightleftarrows O+OH$	2.65E+16	-0.67	17041
5. $O+H+M \rightleftarrows OH+M$	5.00E+17	-1.00	0
6. $2O+M \rightleftarrows O_2+M$	1.20E+17	-1.00	0
7. $O+CO \rightleftarrows CO_2$	1.80E+10	0.00	2385
8. $H+OH+M \rightleftarrows H_2O+M$	2.20E+22	-2.00	0
9. $N+NO \rightleftarrows N_2+O$	2.70E+13	0.00	355
10. $N+O_2 \rightleftarrows NO+O$	9.00E+09	1.00	6500
11. $N+OH \rightleftarrows NO+H$	3.36E+13	0.00	385
12. $SiO+O_2 \rightleftarrows SiO_2+O$	2.31E+13	0.00	26016
13. $SiO+OH \rightleftarrows SiO_2+H$	1.80E+10	0.78	1218
14. $SiO_2 \longrightarrow SiO_2(s)$	2.00E+15	0.00	0

---

[1] This reaction kinetics are optimized to achieve the results for case-8 below

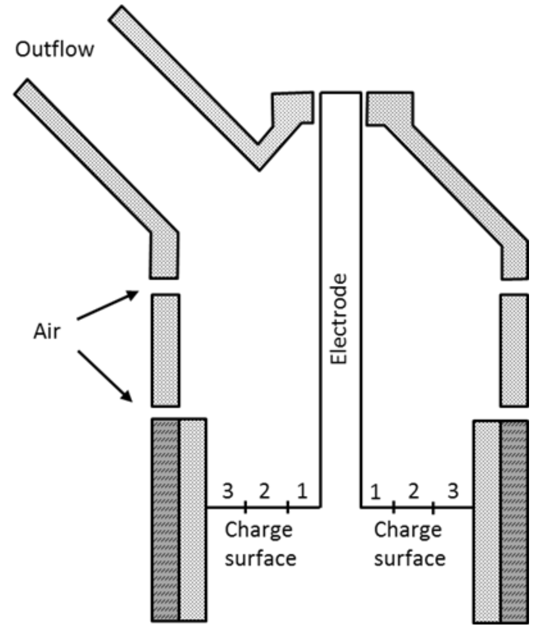

Boundary conditions:
Outlet: pressure outlet
Charge surface: based on tuning with outlet conditions
  Mass flow and gas composition
  70 % inner zone (1)
  20 % middle zone (2)
  10 % outer zone (3)
  Temperature
Electrodes: wall with given temperature
Surroundings: air mass flow inlet
  Mass flow based on tuning with outlet conditions
  Temperature (typical furnace hall temperature)
Walls with external domain: coupled temperature calc.
  Solid walls: material properties
  Thin walls: material properties and specified thickness
Walls with no external domain:
  Thin walls with material properties, specified thickness, heat transfer coefficent and external temperature

Figure 11: Boundary conditions exemplified on pilot scale furnace with 1 electrode

3.2 Boundary conditions and numerics

Choosing the correct boundary conditions for furnace hood simulations requires experience and knowledge about the furnace process. Most of the required boundary conditions are not measured for input to models, and are thus subject for qualified estimation based on experience. An important boundary condition is the amount of process gas arriving through the charge surface into the furnace hood. Since the metallurgical process below the charge surface is not considered in the model, this is a priori unknown to the model. The known parameter is the mass flow through the off-gas channel. This is normally monitored together with the gas temperature. The mass flow of process gas and its temperature through the charge surface is thus estimated by tuning these values such that the measured mass flow and temperature in the off-gas channel is matched. The composition of the process gas is decided by a mass balance based on the measured composition in the off-gas channel and well-known composition of air from the surrounding. Since molecules containing C and Si are introduced by the process gas, the measured amounts of CO, CO_2 and SiO2 will give the amount of CO and SiO in the process gas. Normally most of the process gas is produced close to the electrode and it decreases away from the electrode. The charge surface area is thus divided into three zones, the inner zone closer to the electrode, the middle zone and outer zone. 70% of process gas is emitted through the inner zone, 20% in the middle and remaining 10% at outer zone.

At first glance the tuning procedure for the boundary conditions on the charge surface might seem like cheating since it is tuned to match known results at the outlet which is supposed to be the output of the model and not known a priori. However, this is the only point at which we know the gas composition, its temperature and flow rate. The simulations still provide additional information on local conditions in the furnace hood. The most valuable output of the model, is its capability to predict changes in temperature, pressure drop and NOx emission due to changes in design and operations compared to a base case towards which the model is tuned.

Other boundary conditions are the electrode temperature, heat transfer coefficients, and amount of air and its temperature being sucked into the furnace hood. Normally the surrounding exterior around the furnace hood is included in the computational domain to calculate the distribution of air through different openings. It can normally not be assumed that this is evenly distributed on all openings. Further up in the off-gas channels, the channel walls are boundaries at which heat transfer coefficients and external temperature are specified. This varies whether water cooling is applied, a refractory material is coated on the inside or a simple steel wall is applied.

The differential equations and boundary conditions are solved in a steady state mode with standard velocity-pressure coupling. The equations are solved with first order schemes. Convergence is normally slow. Simulations are considered converged when the temperature in chosen monitoring points have reached a constant value.

3.3 Modelling results

A series of simulations have been conducted for the pilot scale furnace of which experimental data are available. The furnace is illustrated in Figure 12 and vigourosuly described by Solheim *et.al.* [1]. The typical dimensions are 1 m diameter and 1.5 m height of furnace hood. Two sets of circular holes on the furnace hood can be opened and closed to vary the air supply. One set is positioned close to the outlet (upper rings) and one set is positioned closer to the charge surface (lower rings). A computational grid of 1 million polyhedral cells was created for the geometry as seen in Figure 13. A series of tapping cycles were conducted with different variations of air supply and charge material in the experiments as described above. Simulations were performed for 4 different tapping cycles with different operations. It was noted from the experimental data that NOx emissions peak significantly during so-called *blows*. A blow is an incident where a crack in the charge opens up and high amounts of SiO gas is released. Figure 14 shows the variation of NOx, SiO_2, temperature and flow rate during a tapping cycle. We see that NOx emissions correlate with SiO_2 concentrations, and thus SiO blows. Due to the steady-state nature of the modelling concept, we have chosen to compare with the normal operation and filter out the blows in our model validation.

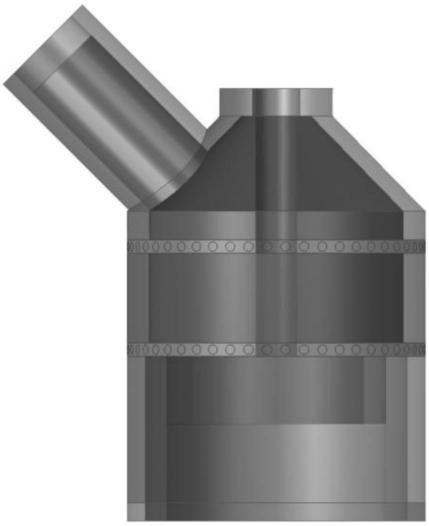

Figure 12: Furnace geometry

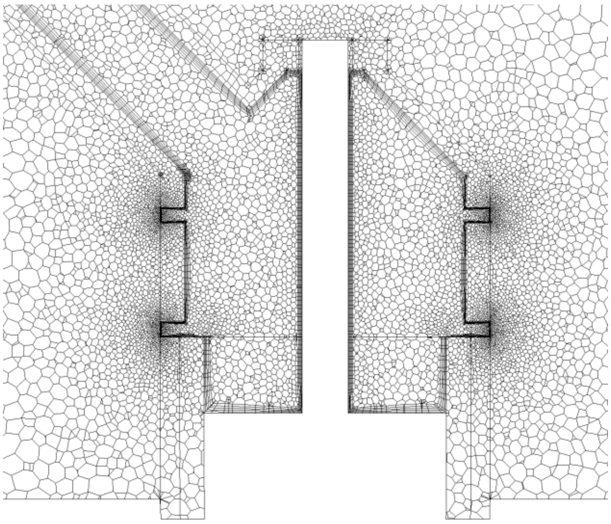

Figure 13: Computational grid

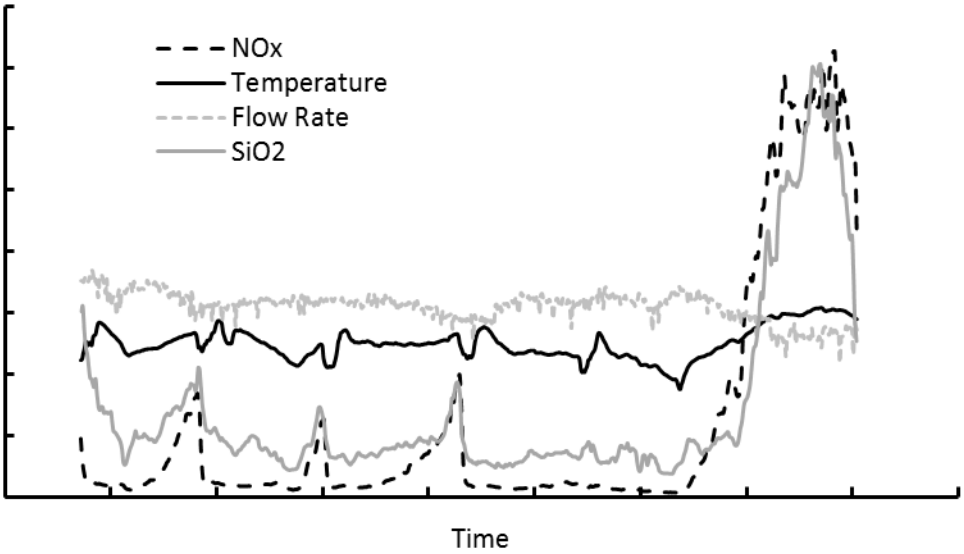

Figure 14: Typical process variations measured in the off-gas channel during a tapping cycle of roughly 1 hour

The simulations were run with standard material properties for ideal gas given by the gas composition. The absorption coefficient in the radiation model is a function of CO2 concentration as given by the wsggm-model. The refractory materials are typical for sintered sand (light grey fields in Figure 11) with k=1.5, and for concrete (textured fields) with k=0.3. The conditions at the mass inlet on the charge surface are seen in Table 8 for the four different cases studied. The values have been obtained by tuning towards the known parameters in the off-gas channel applying the reduced scheme.The air injected in the surrounding area has a temperature of 25°C and a a flow rate covering the difference between the outlet flow rate (off-gas flow rate) and the charge surface flow rate.

Table 8: Case description and charge surface boundary conditions for ideal/normal operations

Conditions		Case			
		6	7	8	11
	Charge	dry	wet	dry	wet
	Upper rings	closed	open	open	closed
	Lower rings	open	closed	closed	open
Off-gas measurements	Flow rate - Nm^3/hr	4500	4430	3897	5470
	Temperature - °C	90	124	118	128
	SiO_2 - %	0.05	0.081	0.084	0.18
	O_2 - %	20.78	20.38	20.6	20.45
	CO - ppm	55	44	40	40
	CO_2 - %	0.43	0.76	0.65	0.73
	NOx - %	4.68	15.1	7.6	17.48
Charge surface	Flow rate - Nm^3/hr	17.5	35	17.5	44
	Temperature - °C	1000	1000	1000	1000
	H_2O - %	0.05	0.2	0.05	0.2
	CO - %	0.8	0.72	0.8	0.62
	SiO - %	0.15	0.08	0.15	0.18

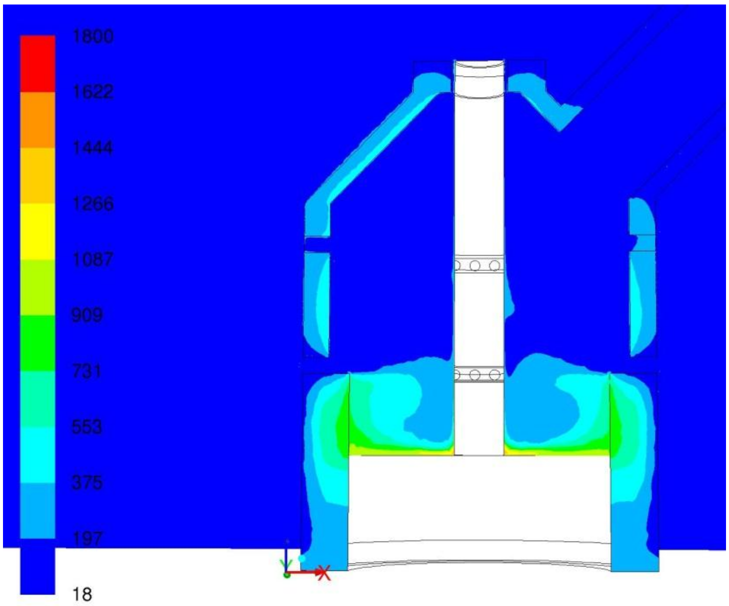

Figure 15: Temperature field (^{o}C) for Case 6 (dry charge, closed upper ring, open lower ring)

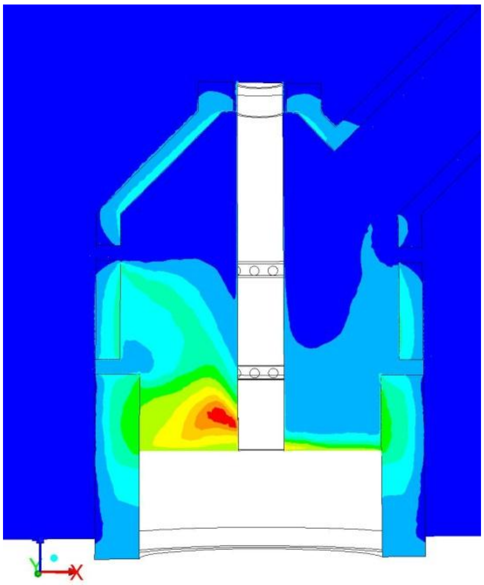

Figure 16: Temperature field (^{o}C) for Case 7 (wet charge, open upper ring, closed lower ring)

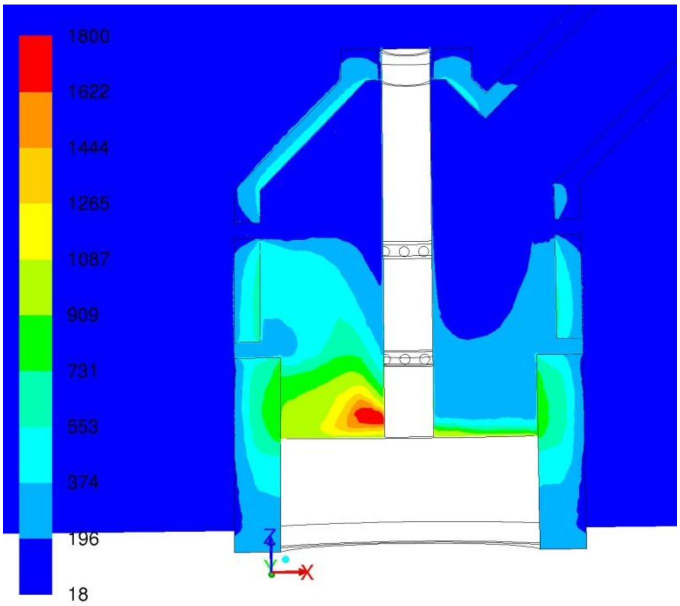

Figure 17: Temperature field (^{o}C) for Case 8 (dry charge, open lower ring, closed lower ring)

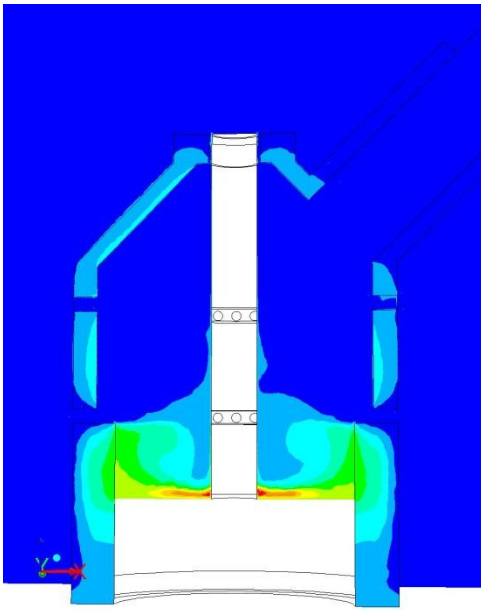

Figure 18: Temperature field (^{o}C) for Case 11 (wet charge, closed upper ring, open lower ring)

From simulations based on he reduced reaction scheme we obtain temperature fields as seen in Figure 15-Figure 18.We see that the cases with open upper rings are warmer with a distinct hot zone above the charge surface on the opposite side of the off-gas outlet. This is explained by lack of cooling air from the lower ring. The air supply from the upper ring loses its cooling effect due to longer residence time before it is mixed with process gas. The asymmetry due to the off-gas outlet, is particularly seen in the temperature field of case 7 and 8 with closed lower rings. This assymmetry is also seen in the O_2 concentration.

Figure 19-Figure 22 show velocity vectors colored by O_2 concentration. We see how air and O_2 is supplied trough the upper or lower rings and the gap around the electrode. With air supplied at the upper rings, less cold air reaches the charge surface and a warmer zone is thus achieved above the surface.

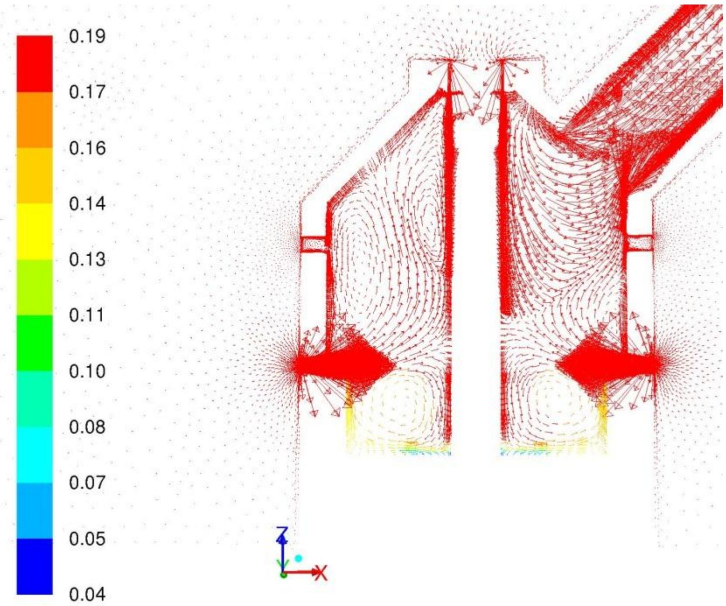

Figure 19: Velocity vectors colored by O_2 concentration for Case 6 (dry charge, closed upper ring, open lower ring)

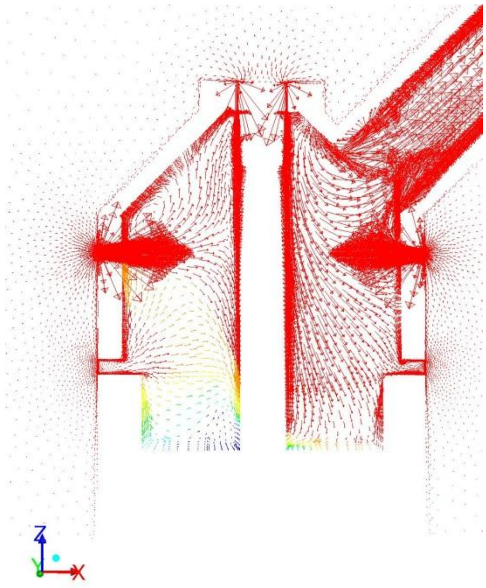

Figure 20: Velocity vectors colored by O_2 concentration for Case 7 (wet charge, open upper ring, closed lower ring)

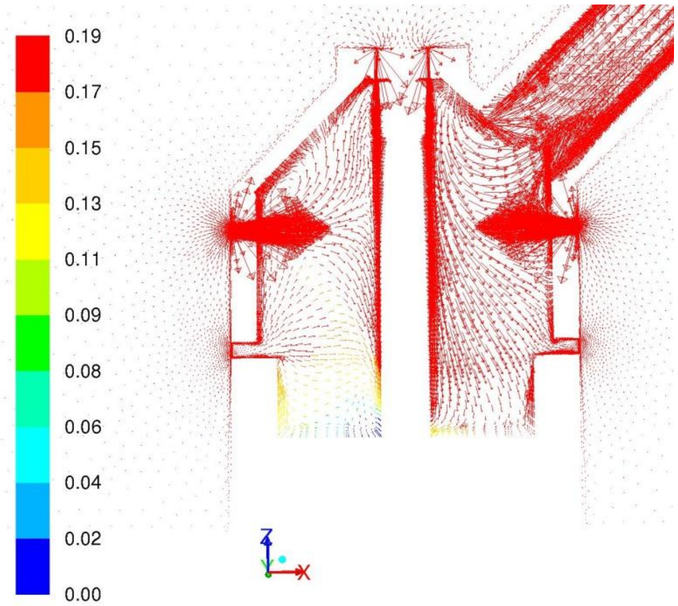

Figure 21: Velocity vectors colored by O_2 concentration for Case 8 (dry charge, open lower ring, closed lower ring)

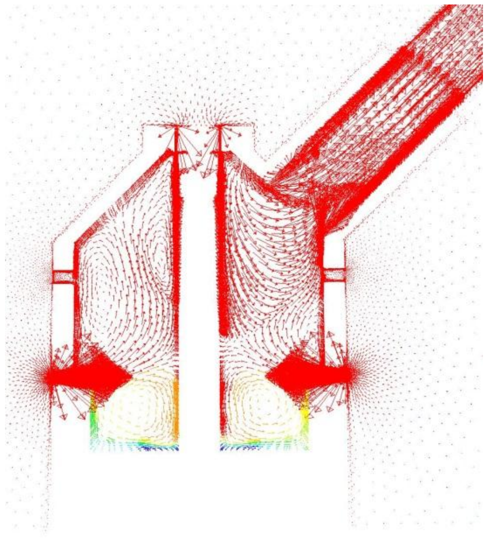

Figure 22: Velocity vectors colored by O_2 concentration for Case 11 (wet charge, closed upper ring, open lower ring)

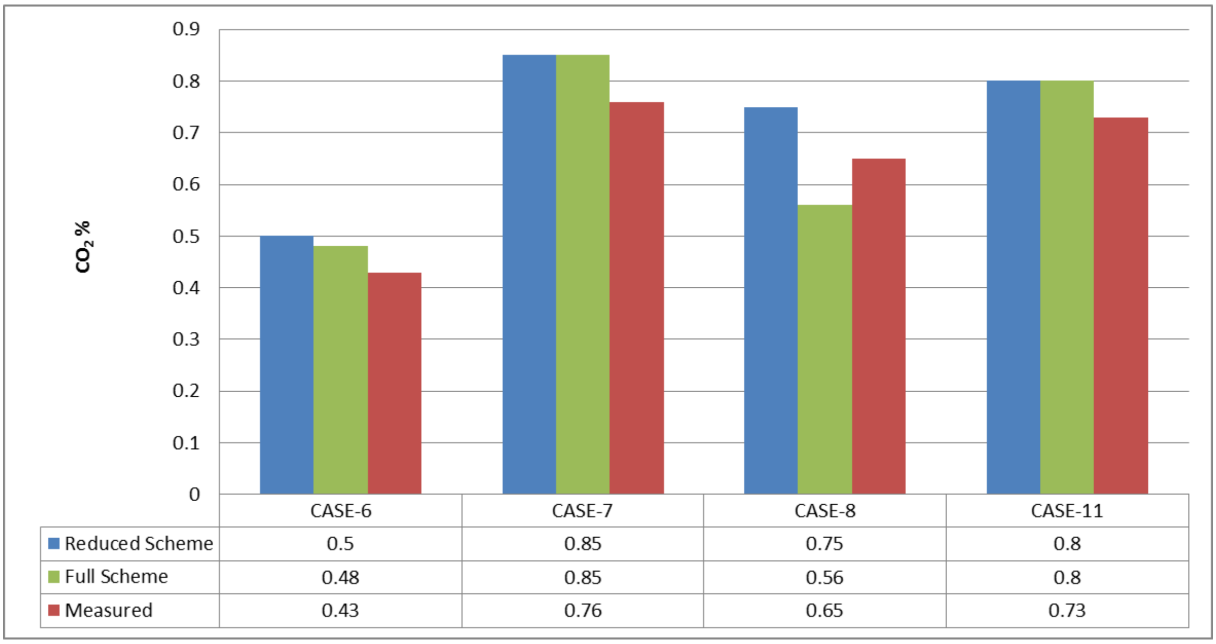

Figure 23: CO_2 concentration in off-gas channel as measured and predicted by models.

Figure 23 shows the measured and predicted levels of CO_2 concentration in the off-gas channel. There is good consistency between experiements and calculations, both for reduced reaction scheme and full scheme. Although there is tuning with regards to the C-atoms, this does not involve the split into CO and CO_2. Thus we may conclude that the models predict the combustion quite well. This is also seen in Table 9 where R2 values are given for prediction of chosen elements in the off-gas channel. Note that it may look as if the reduced scheme performs better than the full scheme. This is not true since the tuning was performed for the reduced scheme, and it thus has a better foundation for predicting the results.

Table 9: R^2 values for model predictions of off-gas composition.

	SiO_2	CO_2	O_2
Reduced scheme	0.98	0.99	0.96
Full scheme	0.98	0.80	0.88

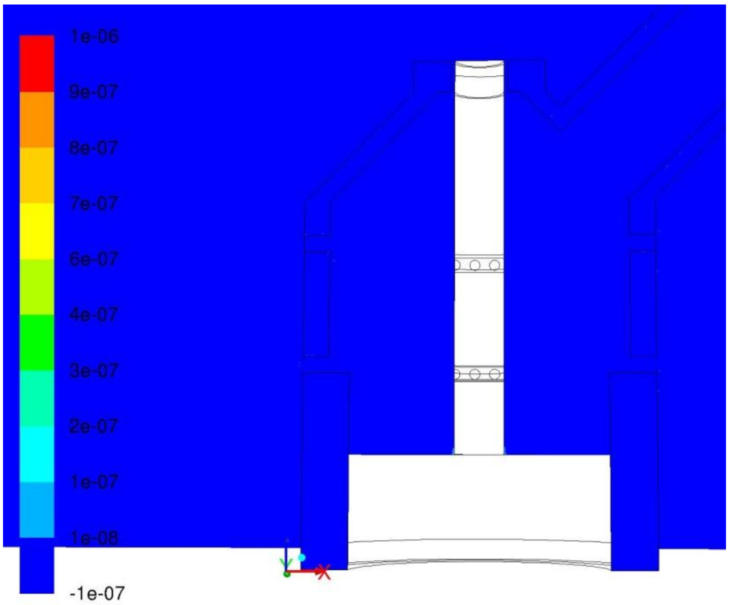

Figure 24: NO formation rate for Case 6 (dry charge, closed upper ring, open lower ring)

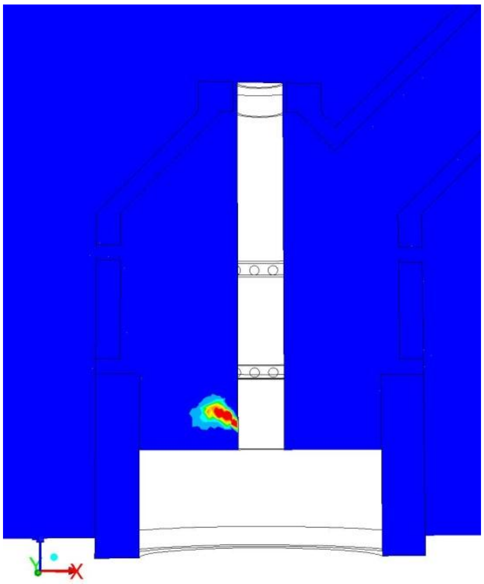

Figure 25: NO formation rate for Case 7 (wet charge, open upper ring, closed lower ring)

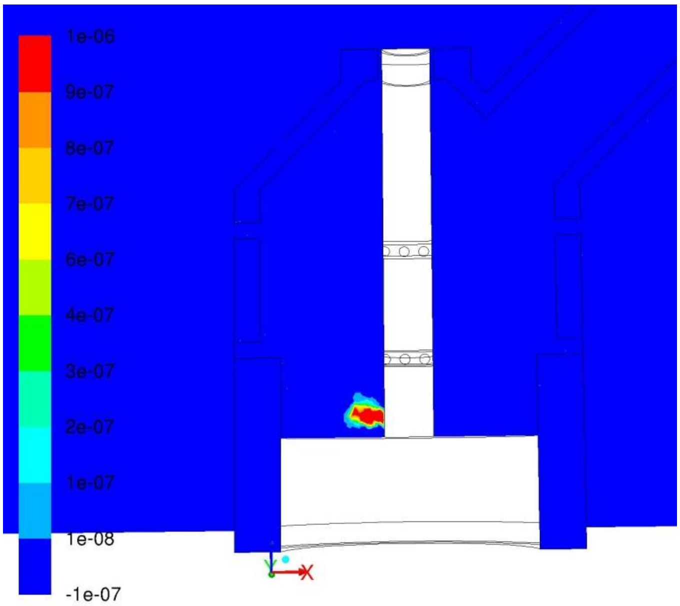

Figure 26: NO formation rate for Case 8 (dry charge, open upper ring, closed lower ring)

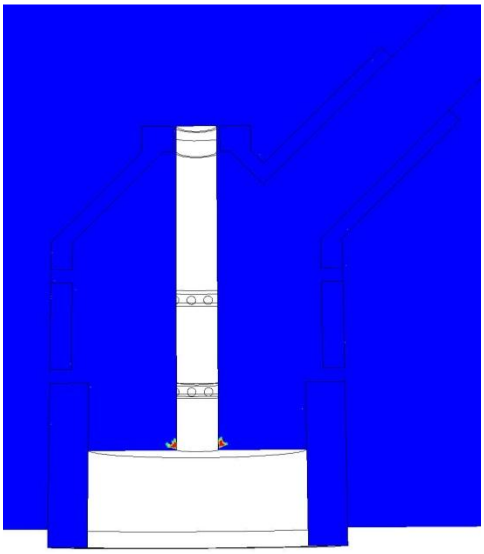

Figure 27: NO formation rate for Case 11 (wet charge, closed upper ring, open lower ring)

The formation rate of NO is seen in Figure 24-Figure 27. We clearly see how the NOx formation correlates with high temperatures which is found in the exact same locations as the NO. When it comes to estimating the NOx emission, the model is not very accurate. The NOx-formation based on a reduced scheme with post-processing of NOx with a turbulence model gives estimates in the right order of magnitude, while the two other approaches underestimates the NOx level with roughly 2 orders of magnitude. This is seen in Figure 28. Even for the post-processing turbulence approach, the estimate is clearly overpredicted. This model is generaly known to overpredict the NOx formation.

Even if the NOx estimation is apparently poor, we also see that all models predict the trend correctly. There is higher NOx levels for the wet charge, and higher NOx levels with open upper rings for the dry charge. Thus the described modelling approaches can not be used for exact NOx estimations, but can be used to predict the effect of design and operation changes on whether NOx emissions will increase or decrease. Certain features should be verified in order to obtain a more accurate NOx model. They include the following:

- Injection of SiO gas in concentrated pockets. This will create higher local temperatures and propably increase NOx-formation
- Include $SiO+H_2O \rightleftarrows SiO_2+H_2$ in the reaction schemes.
- Concider a transient modelling concept with LES turbulence model and flamelet combustion model.

The updated reaction schemes should consider the inclusion of $SiO+H_2O \rightleftarrows SiO_2+H_2$. Currently the reaction kinetics are not known, but the maximum rate is limited to A_r = 2.13E+03 cal/mol, n = 2.5 and E_r = -1207 cal (see Appendix A). A sensitivity analysis should be performed, and if the inclusion of this reaction seems to be of importance, proper reaction kinetics should be obtained. More proper reaction kinetics for SiO2(g)→SiO2(s) should also be considered. The currently used value is a maximum rate.

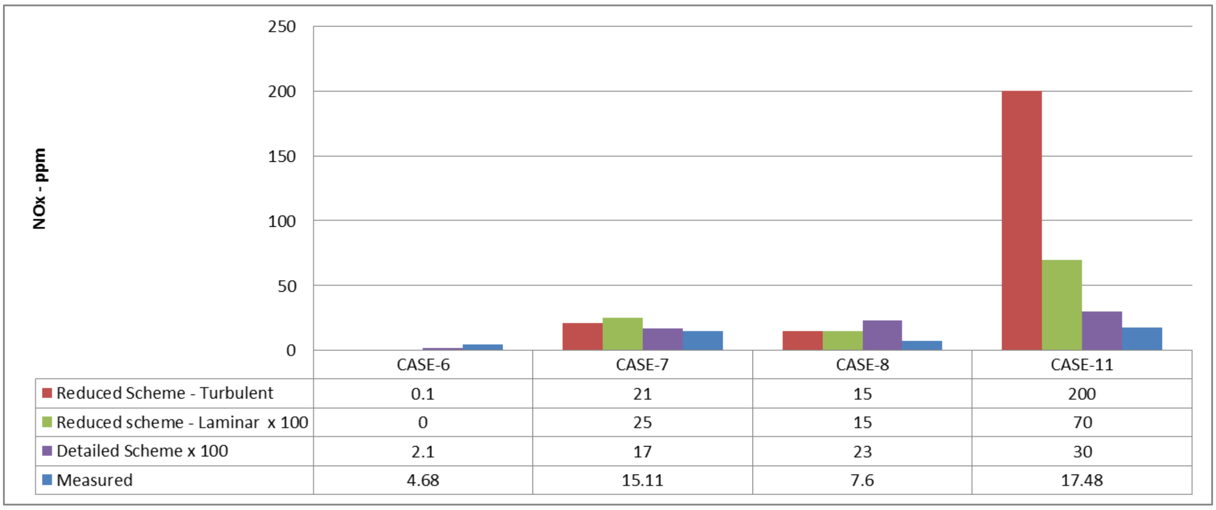

	CASE-6	CASE-7	CASE-8	CASE-11
🟥 Reduced Scheme - Turbulent	0.1	21	15	200
🟩 Reduced scheme - Laminar x 100	0	25	15	70
🟪 Detailed Scheme x 100	2.1	17	23	30
🟦 Measured	4.68	15.11	7.6	17.48

Figure 28: NOx concentration in off-gas channel as measured and predicted by models. Note that some values have been multiplied by 100 for visualization.

4 CONCLUSIONS

Pilot scale experiments were conducted on the one phase pilot furnace of SINTEF. The NOx emission seems to decrease significant by using wet raw materials (charcoal and wet wood chips), compared to using dry raw materials (coke and dry wood chips). This is probably due to addition of both water and hydrocarbons in the gas above the charge. The water evaporation will contribute to decrease the gas temperature. The hydrocarbons will probably consume the oxygen for other competing reactions.

The data from the experiment was used as validation data for a modelling concept describes above. Both a reduced reaction scheme and a full reaction scheme have been assessed. The comparison shows that the model predicts combustion characteristics such as temperature field and gas composition of major species fairly well. Estimation of NOx formation is quantitatively poor for all modelling schemes investigated. However, all trends are picked up by the model. Thus the NOx calculations can be used for assessment of design changes. The model can be improved by considering more realistic boundary conditions, a transient model concept and/or improved reaction schemes. Various potential reactions with SiO have been assessed. It is shown in Appendix A that reactions with CO or CO_2 are not favourable. However, $SiO+H_2O \rightleftarrows SiO_2+H_2$ should be considered in future work.

REFERENCES

[1] Solheim, I., Jensen, R., and Kamfjord, N. E., 2012, "Equipment for Pilot Scale Experiments of Nox-Emissions from the Silicon Process," eds., Orlando, pp.

[2] Pope, S. B., 2000, *Turbulent Flows*, Cambridge University Press, Cambridge, U.K. ; New York.

[3] Chui, E. H., and Raithby, G. D., 1993, "Computation of Radiant Heat Transfer on a Non-Orthogonal Mesh Using the Finite-Volume Method," Numerical Heat Transfer, Part B, 23(pp. 269-288.

[4] Magnussen, B. F., and Hjertager, B. H., 1977, "On Mathematical Modeling of Turbulent Combustion with Special Emphasis on Soot Formation and Combustion," Symposium (International) on Combustion, 16(1), pp. 719-729.

[5] Hanson, R. K., and Salimian, S., 1984, Combustion Chemistry, Survey of Rate Constants in H/N/O Systems.

[6] Westenberg, A. A., 1971, "Kinetics of No and Co in Lean, Premixed Hydrocarbon-Air Flames," Combustion Science and Technology, 4(1), pp. 59-64.

[7] Baulch, D. L., and Et.Al., 1992, "Evaluated Kinetic Data for Combustion Modelling," J.Physical and Chemical Reference Data, 21(3), pp. 441-765.

[8] Smith, G. P., Golden, D. M., Frenklah, M., Moriarty, N. W., and Eiteneer, B., http://www.me.berkeley.edu/gri_mech

[9] Panjwani, B., Andersson, S., and Midtdal, H. F., 2011, "Effect of Sio Combustion on Nox Emissions," eds., Trondheim, pp.

A Evaluation of the feasibility of reactions involving SiO

A.1 Previous work

Previous studies of the kinetics and thermodynamics of reactions of SiO with other gas phase species have involved studies of the following reactions [1,2,3]:

$$SiO + O_2 \rightleftharpoons SiO_2 + O \quad \text{(A.1)}$$

$$SiO + OH \rightleftharpoons SiO_2 + H \quad \text{(A.2)}$$

Since there is an almost complete lack of experimental data, except for one study of these reactions at room temperature [4], it was decided to study these reactions using molecular simulation techniques. Methods that were used to study these reactions were quantum chemical electronic structure calculations that allow for the calculation of the enthalpies and free energies of reaction as well as, e.g., activation energies directly from quantum mechanics without any empirical input. Typical calculations involve the highly accurate, but computationally expensive, coupled cluster methods and the more computationally affordable Density Functional Theory (DFT) methods, which need to be tested against benchmark calculations and/or experiments to test their validity for a given reaction [2]. Reaction rate constants have been calculated using a set of methods based on statistical mechanics, quantum mechanics, and/or classical mechanics, e.g., Molecular Dynamics techniques and Transition State Theory [3]. If care is taken in the choice of methods one should be able to achieve *chemical accuracy*, which means a maximum error of 1 kcal/mol (=4.184 kJ/mol) in the energetics of the reactions. This generally requires lengthy quantum chemistry calculations (on the order of weeks for a job run in parallel). At room temperature chemical accuracy means that any estimated rate constants are of the correct order of magnitude. For higher temperatures the uncertainty in the estimated kinetics typically decreases rapidly.

For reaction (A.1) we were able to calculate the rate constant of reaction using a combination of DFT, using the M06 density functional benchmarked against high-level coupled-cluster calculations, and Transition State Theory [1]. The molecular structures that are used as input into the quantum chemistry calculations and the corresponding energetics are shown schematically in Figure 1.

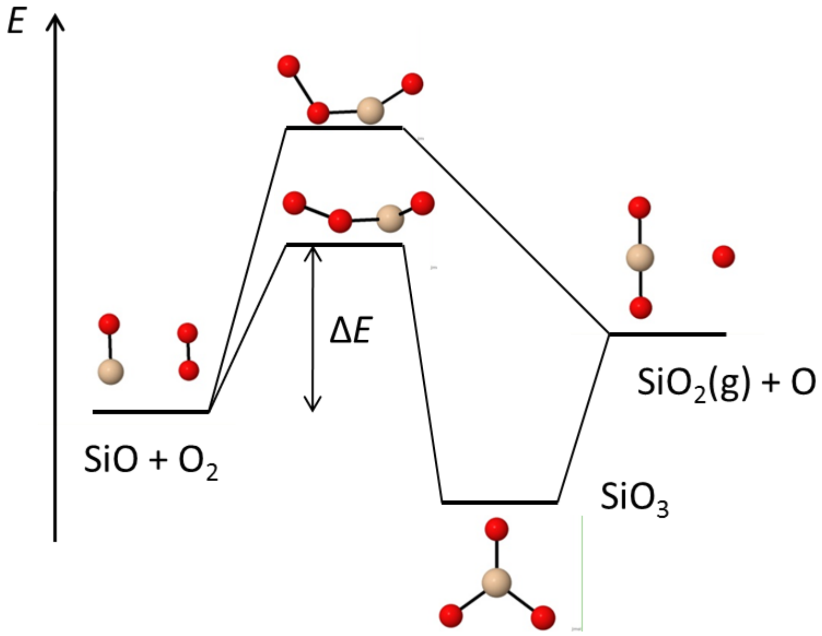

Figure 1. Molecular structures and a schematic view of reaction energetics involved in the $SiO + O_2 \rightleftharpoons SiO_2 + O$ reaction system. Two reaction barriers and the corresponding molecular structures are shown in the middle.

The calculation of rate constants using Transition State Theory is given by the expression

$$k(T) = \frac{k_{\mathrm{B}}T}{h}\frac{Q_{TS}}{Q_R}e^{-\Delta E/k_{\mathrm{B}}T},$$

where k_{B} and h are the Boltzmann and Planck constants respectively, ΔE is the difference in electronic energy between the top of the barrier (Transition State, TS) and the reactant (R), the Q's refers to products of the translational, rotational, and vibrational partition functions. Rotational and vibrational energy levels can be derived from quantum chemical calculations to high accuracy. It is through the partition functions that the effects of atomic motion and thereby entropy are taken into account.

The resulting rate constants are shown in Figure 2 for the relevant temperature range. There is a considerable spread of the estimated rate constants over several orders of magnitude. Our calculated rate constants lie inside the range of rate constants spanned by the estimates and seem to be a more rigorously developed alternative to these previous estimates.

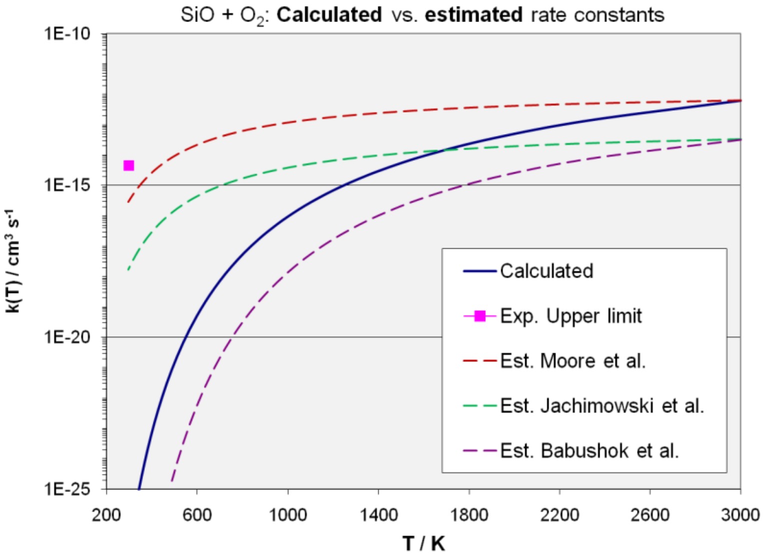

Figure 2. Calculated [1] and estimated reaction rate constants. The experimental value is an upper limit at room temperature as the rate constant was below the detection limit [4]. The estimated rate constants are taken from kinetic models of combustion of silicon species [5,6,7].

For the case of reaction (A.2) above the situation is somewhat more complicated, since there are no clear energy barriers as in the case of reaction (1). This means that Transition State Theory cannot be used as above and other methods are needed. There exist two separate previous calculations of the rate constant of this reaction using *master equation* methods [4,8]. The results of Zachariah and Tsang have been used in this study. These previous simulations [4,8] indicate that the pressure dependence of the rate constant is significant below 1000 K.

We have run DFT and coupled cluster calculations as for reaction (1) and results show that we can expect chemical accuracy for the calculation of rate constants [2]. The M06 density functional has been used as a basis for developing a Potential Energy Surface for the SiO + OH $\rightleftharpoons$ SiO_2 + H reaction system. This allows for the dynamics, and thereby kinetics, of both the forward and reverse reactions to be studied with explicit dynamics calculations. In our case we have run classical trajectory simulations where the reaction is simulated using classical dynamics following the motion of the individual atoms in the collisions and possible reactions of SiO and OH or SiO_2 and H [3]. Through this procedure we have arrived at an estimate of the low-pressure rate constants at a few temperatures. These are shown in Figure 3. As can be seen the comparison with experiments and is rather favorable and support the use of results from the previous calculations by Zachariah and Tsang [8]. Our calculations underestimate the only experimental value (at room temperature and low pressure) by a factor 3 or 4. This type of deviation can be expected (see the discussion on chemical accuracy) above and the deviation from experiments should be smaller at higher temperatures. In order to estimate the pressure dependence of the reaction, the present dynamics calculations will be supplemented by master equation calculations [3]. The results should be the most accurate theoretical estimate of the rate constants of reaction (2) to date.

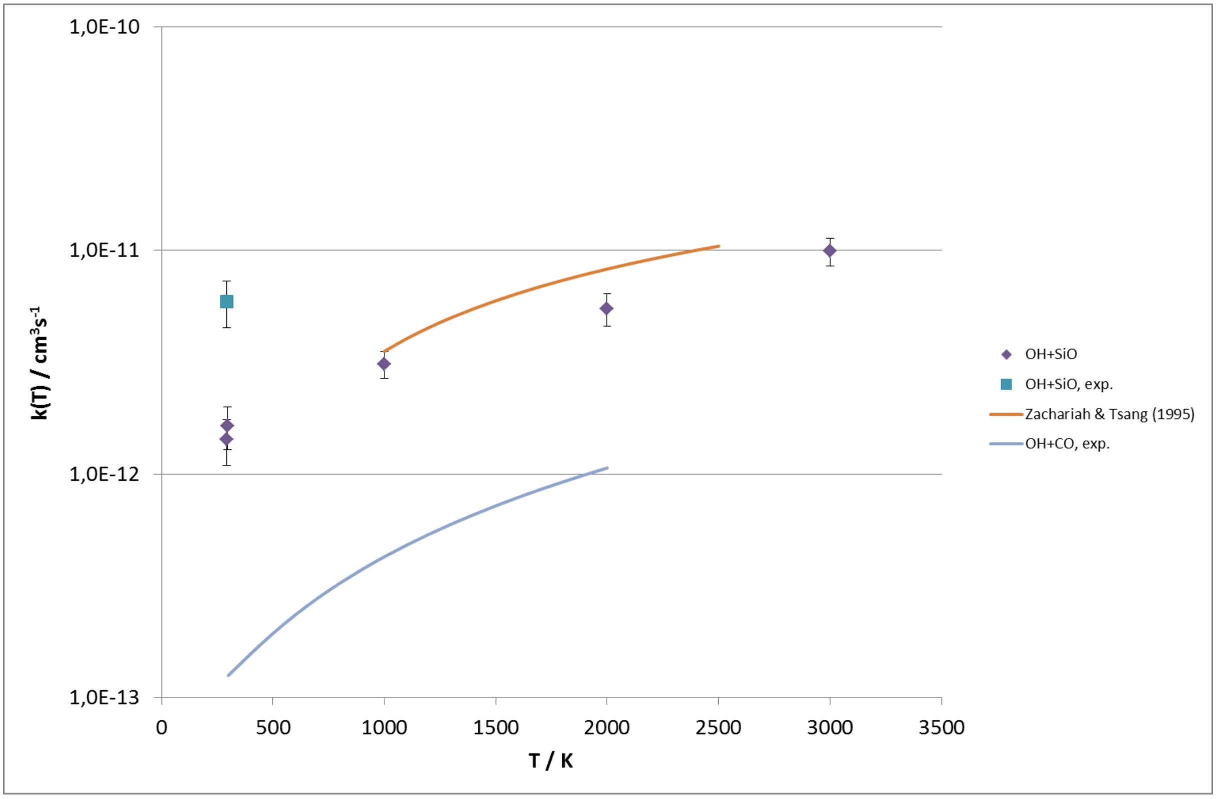

Figure 3. The rate constants of the SiO + OH → SiO_2 + H reaction from our calculations (diamonds) [3], experiments [4], and previous calculations [8]. For comparison the rate constant for the CO + OH → CO_2 + H reaction is shown [9].

A.2 Feasibility of possible reactions involving SiO

In order to include potentially important reactions involving SiO not previously considered in the reaction scheme, and to exclude others, it was decided to evaluate the thermodynamics and, if necessary, kinetics of these reactions. The following reactions were considered as being potentially important (unless indicated otherwise, SiO_2 refers to the gas phase species, i.e., one *monomer* of SiO_2).

$$SiO + CO \rightleftharpoons SiO_2 + C\ /\ Si + CO_2 \tag{A.3}$$

$$SiO + CO_2 \rightleftharpoons SiO_2 + CO \tag{A.4}$$

$$SiO + CH_4 \rightleftharpoons HOSi + CH_3 \tag{A.5}$$

$$SiO + H_2O \rightleftharpoons SiO_2 + H_2 \tag{A.6a}$$

$$SiO + H_2O \rightleftharpoons Si(OH)_2 \tag{A.6b}$$

Reaction (4b) can then be followed by

$$Si(OH)_2 + Si(OH)_2 \rightarrow H_2(SiO_2)_2 + H_2 \qquad (A.7)$$

$$Si(OH)_2 + H_2(SiO_2)_2 \rightarrow H_2(SiO_2)_3 + H_2$$

$$\ldots$$

$$N\, SiO + N\, H_2O \rightarrow H_2(SiO_2)_N + (N\text{-}1)\, H_2$$

When N becomes very large, as in a SiO_2 particle, reactions (A.6b) and (A.7) can be approximated as (given that the involved reactions are sufficiently efficient):

$$SiO + H_2O \rightleftharpoons SiO_2(l,s) + H_2 \qquad (A.8)$$

Quantum chemistry calculations have been run in a similar way to those described in Section A1. The difference is that initial tests have only focused on the thermodynamics and equilibrium constants of the reactions and therefore there is no need to study any reaction barriers in these calculations, and thereby calculations are only needed for the reactants and products. This simplifies the calculations immensely. Descriptions of these calculations will be reported elsewhere [10]. Here we will only focus on the results.

$SiO + CO \rightleftharpoons SiO_2 + C$ / $Si + CO_2$

The reactions in this system are endothermic by about 700 kJ/mol (formation of SiO_2 + C) and 300 kJ/mol (Si + CO_2). The forward reactions are therefore highly unfavored and will not be of significance under process conditions.

$SiO + CO_2 \rightleftharpoons SiO_2 + CO$

The forward reaction is endothermic by about 100 kJ/mol and could potentially play a role in the reaction scheme. Tests of the activation energies indicate that they are very high (300 kJ/mol) and the reaction rates should therefore be very low. It is questionable whether SiO and CO_2 co-exist to any high degree, since the reactions of SiO with O_2 and OH are much faster than those of CO with the same species and SiO should be consumed before any large portion of CO_2 has been formed. The reverse reaction, that is exothermic, might also be important if concentrations of gas-phase SiO_2 are very low and concentrations of CO are very high. This could be the case at the first steps when SiO starts to be oxidized. The reaction barriers for this reaction are still very high, albeit lower than for the forward reaction, and it is questionable if it is of any real importance.

$SiO + CH_4 \rightleftharpoons HOSi + CH_3$

The forward reaction is endothermic by about 300 kJ/mol and it is highly unlikely that it will play any role in the reaction scheme. If it were there would be a release of highly reactive CH_3 radicals that would significantly alter and complicate the current reaction scheme.

$SiO + H_2O \rightleftharpoons SiO_2(g) + H_2$

This direct reaction is endothermic by 60 kJ/mol and could play a definite role at high temperatures. See Figure 4 for a plot of the equilibrium constant. However both our and previous calculations [11] predict a complex reaction in several steps and a high activation energy. Further investigations of the kinetics of the reaction are necessary, but this is outside the scope of the current project.

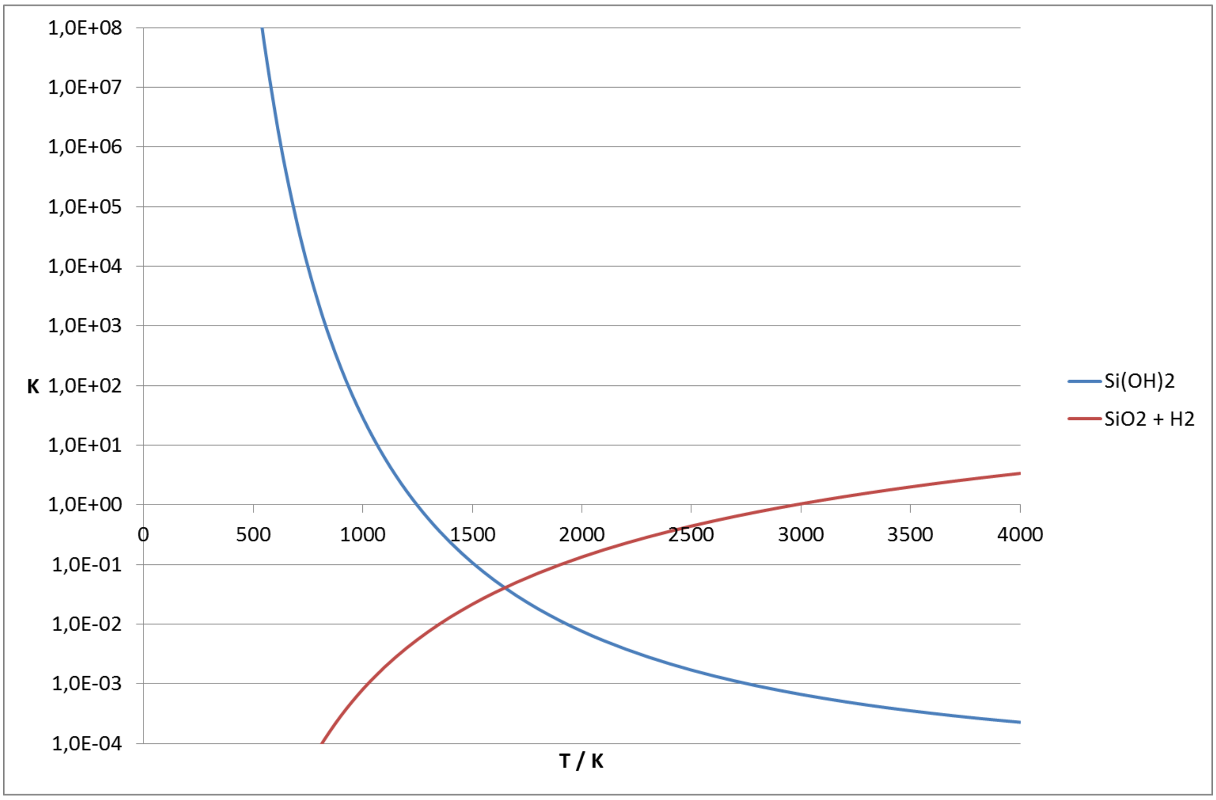

Figure 4. Equilibrium constants of reactions (6a) and (6b).

$SiO + H_2O \rightleftharpoons Si(OH)_2$

This association reaction is exothermic and has a low reaction barrier height, so it could be of importance. What is not clear from this initial survey is the likelihood that $Si(OH)_2$ will react further, before it possibly decomposes back to reactants. As can be seen in Fig. 4 it seems that formation of $Si(OH)_2$ becomes increasingly less favored with increasing temperatures. However, the equilibrium constant is still significant in the whole temperature range. Further studies into the kinetics of this reaction would be highly valuable. A Transition State Theory estimate has been calculated of the rate constant for reaction (A.6a) together with reaction (A.6b) that both eventually give $SiO_2 + H_2$, if reaction (A.7) is efficient. This is shown in Figure 5. This represents an absolute maximum rate of this reaction since it assumes that all collisions leading to $Si(OH)_2$ formation eventually lead to $SiO_2 + H_2$ (reaction (A.8)).

$Si(OH)_2 + Si(OH)_2 \rightarrow H_2(SiO_2)_2 + H_2$

This reaction has several possible products. By plotting the equilibrium constants for all of these (Fig. 6) it becomes clear that condensation into $H_2(SiO_2)_2 + H_2$ is favored at all relevant temperatures. Therefore this is a very interesting potential alternative route to silica dust formation. A simple collision rate constant has been calculated for this reaction (see Fig. 5), but this is not necessarily the same as the total reaction rate constant as many collisions might be non-reactive. More studies into the kinetics of this reaction should be a priority.

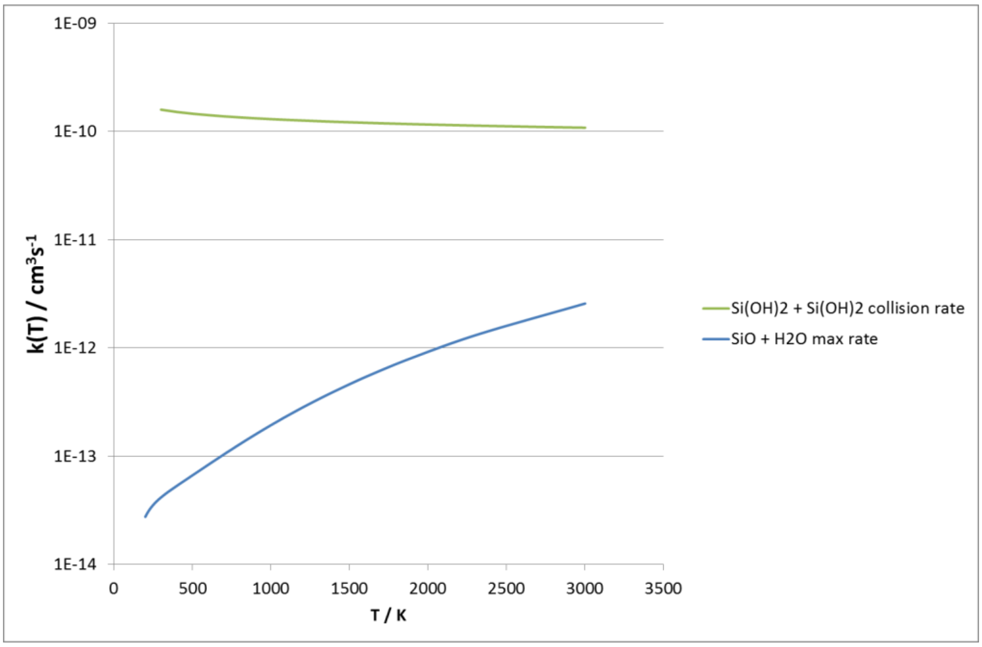

Figure 5. Rate constants for the maximum possible rate constant of reaction (8) together with rate constants for the initial condensation step for $Si(OH)_2$ formation, reaction (7).

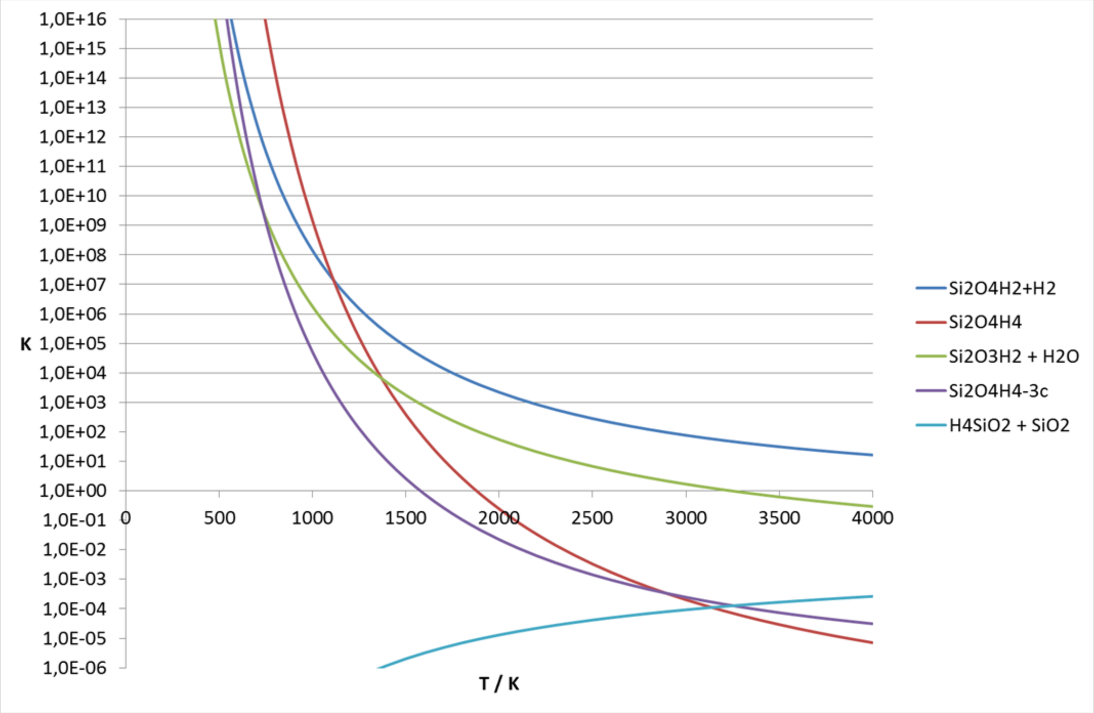

Figure 6. Equilibrium constants for alternative products from the first step of reaction (7).

References

[1] B. Panjwani, S. Andersson, H. Midtdal, 8th International Conference in CFD in Oil & Gas, Metallurgical and Process Industries, Trondheim, Norway, 21 – 23 June 2011.

[2] S. Andersson, R. Valero, *to be published*

[3] S. Andersson, T. J. Frankcombe, R. Valero, *to be published*

[4] Gómez Martín, J. C.; Blitz, M. A.; Plane, J. M. C. *Phys. Chem. Chem. Phys.* **2009**, *11*, 10945–10954.

[5] Moore, T.; Brady, B.; Martin, L. R. *Combust. Flame* **2006**, *146*, 407–418.

[6] Jachimowski, C. J.; McLain, A. G. *Nasa Technical Paper 2129*, 1983.

[7] V.I. Babushok, W. Tsang, D.R. Burgess & M.R. Zachariah, 27th Symp. (Intl.) on Combustion, The Combustion Institute, 2431-2439, 1998.

[8] Zachariah, M. R.; Tsang, W. *J. Phys. Chem.***1995**, *99*, 5308–5318.

[9] NIST Chemical Kinetics Database, http://kinetics.nist.gov

[10] S. Andersson, *to be published*

[11] R. Becerra et al., Phys. Chem. Chem. Phys. 7 (2005) 2900-2908.

SINTEF

Technology for a better society

www.sintef.no